Inelastic Scattering of Slow Neutrons from Methane*

P. D. RANDOLPH, R. M. BRUGGER, K. A. STRONG, AND R. E. SCHMUNK
Atomic Energy Division, Phillips Petroleum Company, Idaho Falls, Idaho

(Received June 15, 1961)

Partial differential cross sections for the scattering of neutrons of 0.0150, 0.0252, 0.0706, 0.103, and 0.142 ev initial energy into angles of 16.3°, 26.0°, 36.4°, 47.6°, 59.5°, 72.1°, and 84.7° from samples of room temperature methane gas are presented. These are converted to scattering law and are compared to three calculations: (1) The ideal gas calculation gives limited agreement using a mass of 3.2, the average of the Sachs-Teller mass tensor; (2) the Krieger-Nelkin approximation which includes effects of zero-point vibrations is a better fit, but underestimates in the region of large momentum transfers; (3) a calculation using exact thermal orientation averages of the matrix elements gives the best fits. None of the calculations explain the results at small energy and momentum changes; this disagreement is attributed to the classical treatment of the rotational states in these calculations.

I. INTRODUCTION

MEASUREMENTS of the partial differential cross sections (differential in scattered neutron wavelength or energy and scattering angle) for slow neutrons scattered from methane gas at room temperature are presented and discussed. These measurements were made, using the MTR (Materials Testing Reactor) phased-chopper velocity selector[1] as the neutron monochromator, at incident neutron energies in the range 0.015 to 0.14 ev.

Previous experimental studies of the interaction of neutrons in the thermal energy range with gases were devoted mainly to the measurements of the energy dependence of the total cross section.[2,3] For methane, the total cross section has been measured by Carrol[4] for cadmium filtered neutrons and by Melkonian[5] as a function of energy in the energy range 0.003 to 3.0 ev using time-of-flight methods. The angular distribution of methane has been measured by Alcock and Hurst[6] at 0.0732 ev using a crystal spectrometer.

Of basic interest in the study of neutron interactions with gases and liquids are the partial differential cross sections. In the thermal energy range where the static and dynamic effects of chemical binding and local order in the material are most pronounced, information about these structural properties may be obtained from their effects on the partial differential cross sections. At thermal energies such cross sections are also important to the neutron moderation process since chemical binding and local order in a material have large effects at these energies. As an early study, during which experimental methods and techniques of data analysis were developed, methane was chosen as the sample material because it is one of the simplest hydrocarbon gases. Also an exact formalism of slow neutron scattering from gases has been developed[7] as have approximate theories[8,9] using the mass tensor of Sachs-Teller[10] which may be compared to experiment. Since the scattering is predominantly incoherent, the problem of distinguishing between coherent and incoherent effects is minimized. The time-of-flight spectra of a gas are broad so that finite instrumental energy resolution does not introduce large errors. Finally, the cross section of hydrogen allows convenient sample sizes to be used.

The experimental method is described in Sec. II and the experimental partial differential cross sections are presented in Sec. III. Section IV is devoted to the scattering law presentation proposed by Egelstaff,[11] with a presentation of the experiment in terms of it. This is a particularly convenient method of presentation since it depends only on the structural properties of the material and also because it compares information obtained from different incident energies and scattering angles. In Sec. V three calculations are compared with the experimental data. The calculations are: (a) The ideal gas,[7] hereafter called IG; (b) a classical rotator calculation of the exact theory of Zemach and Glauber[7] as applied to methane, hereafter called EA[12] (exact averaging); and (c) the Krieger-Nelkin[9] mass-tensor approximation to Zemach and Glauber's theory,[12] hereafter called KN.

II. DESCRIPTION OF THE APPARATUS AND EXPERIMENT

A. Apparatus

A detailed description of the MTR slow-neutron phased-chopper velocity selector and its associated appa-

* Work done under auspices of the U. S. Atomic Energy Commission.

[1] R. M. Brugger and J. E. Evans, Nuclear Instr. **12**, 75 (1961); R. M. Brugger and J. E. Evans, International Atomic Energy Agency Symposium on Inelastic Scattering of Neutrons in Solids and Liquids, Vienna, 1960 [International Atomic Energy Agency (to be published)], paper IS/31.

[2] E. Fermi and L. Marshall, Phys. Rev. **71**, 666 (1947).

[3] E. Melkonian, L. S. Rainwater, W. W. Havens, and J. R. Dunning, Phys. Rev. **73**, 1399 (1948).

[4] H. Carrol, Phys. Rev. **60**, 702 (1941).

[5] E. Melkonian, Phys. Rev. **76**, 1750 (1949).

[6] N. F. Alcock and D. G. Hurst, Phys. Rev. **83**, 1100 (1951).

[7] A. C. Zemach and R. J. Glauber, Phys. Rev. **101**, 118, 129 (1956).

[8] A. M. L. Messiah, Phys. Rev. **84**, 204 (1951).

[9] T. J. Krieger and M. S. Nelkin, Phys. Rev. **106**, 290 (1957).

[10] R. G. Sachs and E. Teller, Phys. Rev. **60**, 18 (1941).

[11] P. A. Egelstaff, Atomic Energy Research Establishment Report AERE-R-3622, 1961 (unpublished); and International Atomic Energy Agency Symposium on Inelastic Scattering of Neutrons in Solids and Liquids, Vienna, 1960 [International Atomic Energy Agency (to be published)], paper IS/P17.

[12] G. W. Griffing and H. L. McMurry, Atomic Energy Commission Report IDO-16692, 1961 (unpublished).

ratus has been given elsewhere.[1] Figure 1 shows a schematic drawing of the velocity selector, its shielding, and detectors. Briefly, it consists of two Fermi-type slow choppers having curved slit inserts and spaced 3.43 m apart, both rotating about vertical axes with the same angular speed (4725 rpm). The first chopper A chops the reactor beam into bursts of polychromatic neutrons which spread out in time as they move down the drift tube to the second chopper D which spins at exactly the same speed as A and has a definite angular phase with respect to A. The angular phase of D with respect to A is adjusted so that D is open at a predetermined time after A is open. Thus D allows neutrons of only one narrow velocity range to pass. Between these two choppers are two phased rotating collimators, B and C, which have no curved slit inserts and whose purpose is to reduce background caused by fast neutrons. The neutron flight path through the reactor beam plug and velocity selector is evacuated; however, the flight paths from the velocity selector to the target and the detectors are in air. The beam size at the exit of the velocity selector is 4 in. high by 1.33 in. wide. The wavelength resolution of the velocity selector for elastically scattered neutrons, $\Delta\lambda/\lambda=\Delta t/t$, where t is the target to detector time-of-flight and Δt is the full-width at half-maximum of the burst, as measured at the detectors, is about 3.5% for 0.015-ev neutrons and about 8% for 0.14-ev neutrons.[1] A 4096-channel time-of-flight analyzer is used to time-analyze and store the information from each of seven detectors. The start trigger for this analyzer is obtained from a magnetic pickup on chopper D.

B. Experimental Procedure

Monoenergetic neutrons from the velocity selector are scattered by the sample and detected by BF_3 counter banks located at seven scattering angles in the range 16° to 84°. An eighth detector, located in the forward beam, serves as a beam intensity and burst shape monitor. The counts detected in each of the eight detectors are recorded as a separate 256-channel time-of-flight spectrum. These data occupy one-half (2048 channels) of the available analyzer storage. Background data obtained using an empty holder in the sample position are stored in the remaining half of the analyzer, again as eight 256-channel spectra. An automatic sample changer cycles the sample and empty sample holder into the beam at ten minute intervals and also switches the detector outputs from the first to the second half of the analyzer. Data runs, normally 48 hr long, were taken at 0.0150, 0.0252, 0.0706, 0.103, and 0.142 ev incident neutron energies using 10-μsec channel widths. Background corrections were made by subtracting the empty holder data from the sample data. These background corrected time-of-flight spectra were then converted, using a computer program, to partial differential cross sections in the forms differential in scattered neutron wavelength

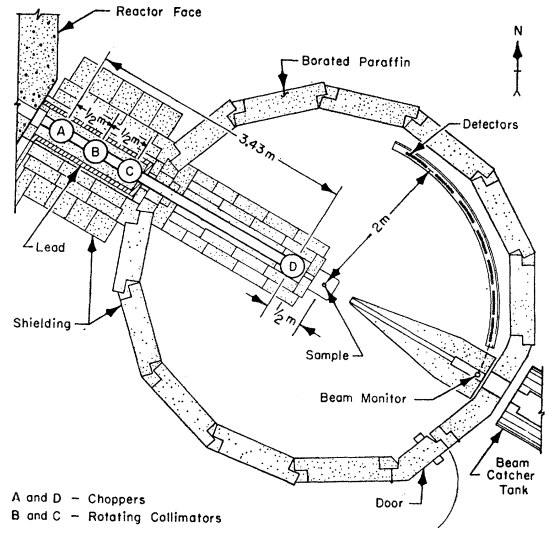

FIG. 1. Schematic drawing, plan view, of the MTR neutron velocity selector and shielding.

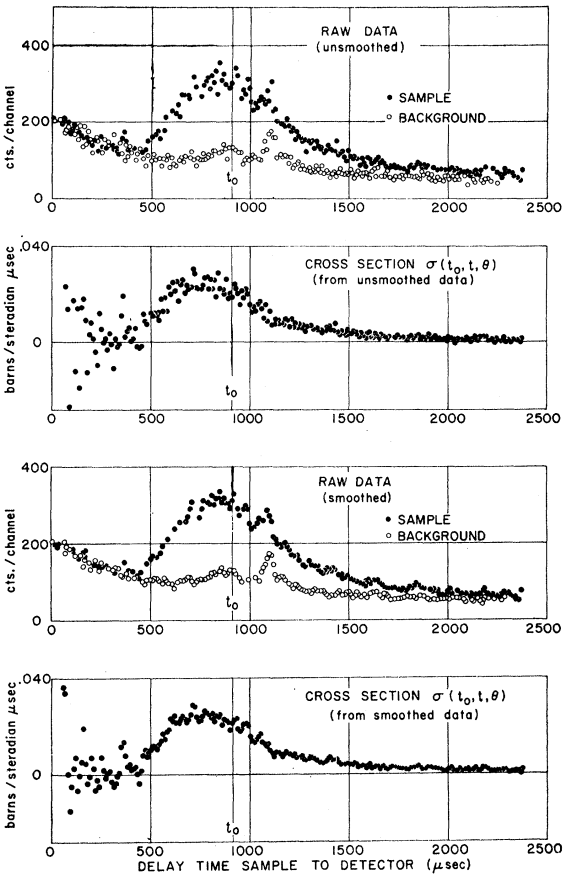

FIG. 2. The effect of smoothing the sample and background data on the partial differential cross section. The data shown are for an incident energy of 0.0252 ev and 72.1° scattering angle with a 1400-min running time each for the sample and background. The partial cross section is per molecule. The time t_0 (915 μsec) is the time for elastically scattered neutrons to travel from the sample to the detector.

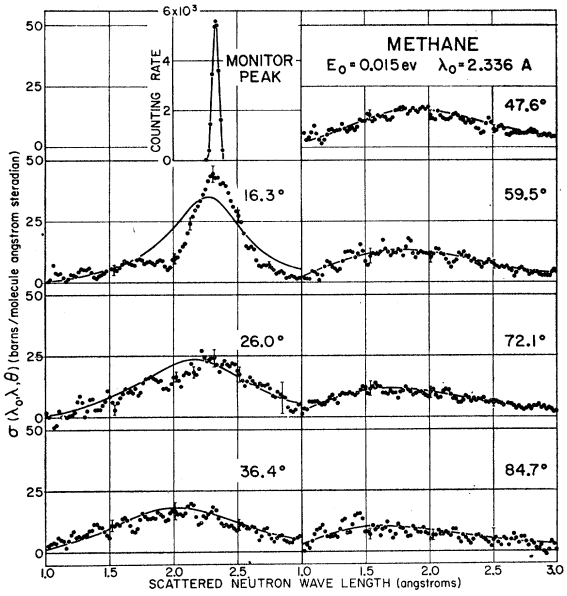

FIG. 3. Partial differential cross sections for scattering 0.0150-ev neutrons from room temperature methane. The apparent structure in the cross section is spurious and is caused by the data smoothing program in fitting the large statistical fluctuations due to low counting rates. The solid curves are the results of the EA calculation (Sec. V).

and angle and also to the form differential in scattered neutron energy and angle.

A detailed discussion of background sources, detector banks, resolution, and the intensity calibrations used to convert to cross sections is given in reference 1.

C. Data Smoothing and Background Corrections

Before background corrections are made both the sample and the empty sample holder data are smoothed. This smoothing is done on the data in each channel of the time-of-flight spectrum. It is accomplished by a computer program which makes a least-squares fit of a parabola to five adjacent data points (40-μsec time-of-flight interval), the data point to be corrected being the middle one. The program then advances one time channel and repeats the process. This procedure introduces little broadening of the experimental resolution since the time-of-flight interval used in the smoothing is about the same as the instrumental burst width at a detector ($\sim$32–36 μsec). The general result of the smoothing process is to reduce the average point spread of the sample and background data and thus also the spread in the corrected time-of-flight spectrum. Over most of the spectrum then, this increases the experimental accuracy at a given point since information from adjacent points is used to establish its smoothed value. However, in a region of the spectrum where a large statistical fluctuation happens to occur (in either background or sample data), the smoothing process can cause such a fluctuation to appear as a spurious extremum which may remain after background is subtracted. For low-density gas samples such as used here, such spurious effects may be safely ignored since no true coherent inelastic scattering events are to be expected and the spectrum is a smooth function having but one maximum. Figure 2 illustrates the effects of the smoothing process on the data from a typical time-of-flight spectrum. The clear appearance of small fluctuations in the smoothed data can be caused by two effects; (a) an actual coherent neutron scattering due to phonon excitation in the aluminum sample holder, and (b) spurious extrema generated by the smoothing process in fitting statistical fluctuations as mentioned above. If such a peak is caused by phonon excitation, it generally appears in both the sample and the empty sample holder data and is then almost completely removed when background is subtracted. An example of this is seen at $\sim$1150 μsec in Fig. 2. No correction is made for the spurious extrema in making the background subtraction. The error in the cross section caused by ignoring these is then no larger than the original statistical error in the data. The large point scatter in the cross section at short delay times is due to the background subtraction, where the difference in the number of counts is small compared to the numbers subtracted. This point spread is further increased in the conversion to cross section when the detector efficiency is taken into account.

D. Samples

The methane samples used were "pure grade" of 99% mol purity. The impurities in the sample were: 0.12% ethane, 0.03% propane, 0.60% N_2, and 0.20% CO_2.[13]

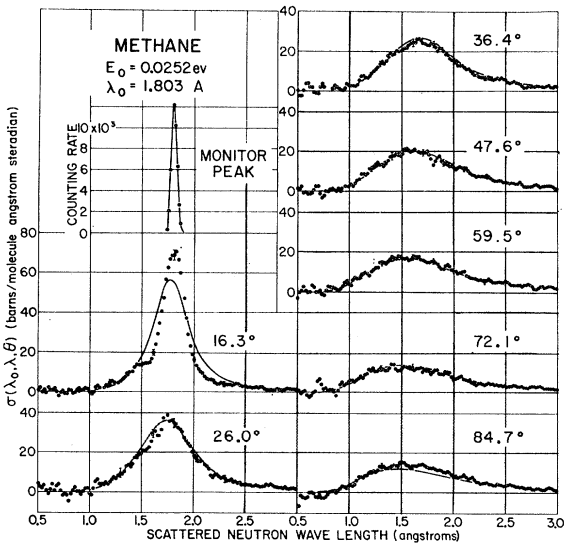

FIG. 4. Partial differential cross sections for scattering 0.0252-ev neutrons from room temperature methane. The solid curves are the results of the EA calculation (Sec. V).

[13] J. C. Hillyer, Special Products Division, Phillips Petroleum Company, Bartlesville, Oklahoma (private communication).

The effects of these impurities on the scattering is negligible since the ethane, which has the largest effect, contributes only 0.2% to the total scattering. The sample holders are circular cylinders constructed of 2.25-in. o.d., 0.062-in. wall, 61S-T aluminum tubing. The portion of the cylinder in the beam was machined as thin as feasible for the pressures used. For 0.015 and 0.025 ev, walls of 0.010-in. thickness were used with filling pressures of 45 and 50 psig, respectively. At 0.07, 0.10, and 0.14 ev, walls of 0.030-in. thickness were used at pressures of 64, 100, and 100 psig, respectively. The pressures are such as to give approximately 90% transmission. These cylinders are mounted with their axes perpendicular to the scattering plane. The empty holders were evacuated cans of identical construction and wall thickness. The amount of gas in each cylinder was determined by weighing both before and after filling. The samples were weighed also after each data run, and no leakage was observed. The effective sample thickness, determined by averaging the path distance through the cylinder over the width of the beam (1.33 in.), was 5.03 cm. No special care was taken to control the sample temperature since the normal scattering room temperature is 21±2°C.

The effects of multiple scattering within the sample are difficult to estimate, since to make accurate calculations, the partial differential cross section and a complex computer program are required. If the assumption is made that the double scattering has the same angular dependence as the elastic scattering, a crude calculation

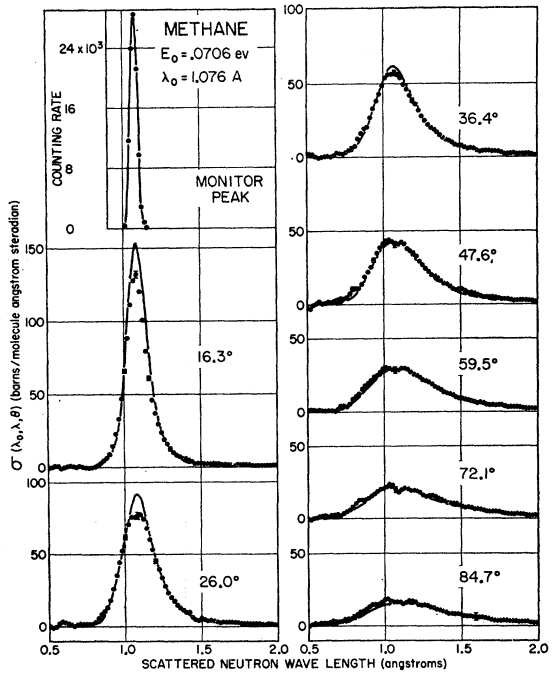

FIG. 5. Partial differential cross sections for scattering 0.0706-ev neutrons from room-temperature methane. The solid curves are the results of the EA calculation (Sec. V).

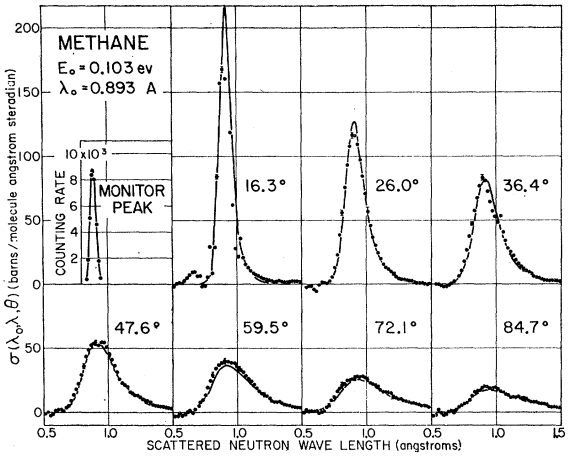

FIG. 6. Partial differential cross sections for scattering 0.103-ev neutrons from room-temperature methane. The secondary peak seen in 16.3° spectrum at short wavelengths is spurious. It is due to a loss of background data caused by a trouble in the core storage matrix of the time-of-flight analyzer. The solid curves are the results of the EA calculation (Sec. V).

for the cylindrical geometry indicates that double scattering for these sample thicknesses varies from about 2.5% of the total scattering at 16° to about 3% at 85°. This rough calculation tends to underestimate the effects. On the other hand, applying Vineyard's[14] multiple elastic scattering results to a plane slab whose thickness is the effective cylinder thickness, yields values from 3% at 16° to about 6.5% at 85°, which overestimates the effect. Since these effects are small and the values obtained from rough calculations uncertain, no multiple scattering correction to the data was made. The assumption that multiple scattering does not introduce large errors is confirmed when the data are presented in terms of the scattering law (see Sec. IV).

The finite sample thickness may affect the wavelength resolution of the experiment by the uncertainties introduced in the scattered neutron flight distance. For the sample sizes used, the mean fractional difference in scattered-neutron flight distance for a neutron scattered at the center of the sample, and one scattered somewhere else in the sample, at a fixed scattering angle, is only $\Delta d/d = \Delta\lambda/\lambda \lesssim 0.01$. On the other hand, the experimental resolution for elastically scattered neutrons, which is indicated by the width at half-maximum of the burst shape of the forward beam, $\Delta t/t = \Delta\lambda/\lambda$ varies from 0.035 at 0.015 ev to 0.08 at 0.14 ev. Thus, the sample thickness causes a negligible broadening of the resolution.

III. EXPERIMENTAL RESULTS

The methane partial differential cross sections obtained in this experiment are shown in Figs. 3–7. These show the cross section in barns/molecule (4 hydrogens +1 carbon) angstrom steradian vs scattered

[14] G. H. Vineyard, Phys. Rev. **96**, 93 (1954).

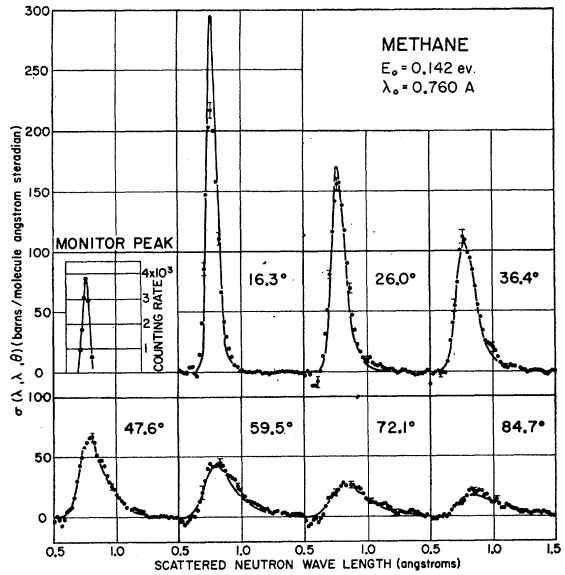

FIG. 7. Partial differential cross sections for scattering 0.142-ev neutrons from room-temperature methane. The solid curves are the results of the EA calculation (Sec. V).

neutron wavelength. The burst shape of the incident beam as measured by the beam monitor is also shown. The representative error flags indicate only the raw data counting statistical errors and are about the same as indicated by the point spread in the data. Generally the signal to background ratio is better for the 0.07 and 0.1 ev initial neutron energy data since the reactor thermal flux is higher at these energies than at the other incident energies. The signal to background ratio is poor at 0.015 ev. The presence of what appear to be slight double maxima in the cross sections, most easily seen near the peak at 0.07 ev in Fig. 5 where the statistics are best, are due to slight differences between the empty sample holder and the blank sample holder. These slight differences cause an incorrect subtraction of the elastic (Bragg) scattering from the aluminum and also of the coherent inelastic scattering (phonon excitation) in the aluminum.

No attempt has been made to remove instrumental resolution from the data. An indication of the resolution is given by the beam monitor burst shapes shown in Figs. 3–7. Since the monitor is located at the same distance from the sample as the detector banks, the wavelength spread at the detectors for elastically scattered neutrons[1] is the same to good accuracy as that in the beam monitor burst. The effect of inelastic scattering on the burst width in time (or wavelength) of the scattered neutrons broadens the energy width of the burst, the largest amount occurring for the highest incident energies. Even at the highest incident energy, 0.14 ev, the resolution $\Delta\lambda/\lambda$ for a 2-m flight path is only increased from a value of 8% to a value of 10% by inelastic scattering.[1] At lower incident energies the maximum widths of the burst of inelastically scattered neutrons are all less than 8%. Since the peak in the cross sections of Figs. 3–7 are all at least twice as wide as the burst for elastic scattering as measured by the monitor, instrumental energy resolution does not have a large effect on the data.

The spread in the scattering angles subtended by each counter bank is $\pm 3.5°$ about the measured scattering angle. Such a spread affects the angular resolution most for forward scattering angles where the cross section changes most rapidly. An estimate of the magnitude of this effect was made by comparing the computed partial differential cross sections (for an ideal gas) at the angles corresponding to the edges of the counter bank with the cross section at the center of the bank. This calculation showed that at 0.025 ev the net deviation of the 16-degree cross section due to contributions from the 12- and 20-degree angles as a function of wavelength of the scattered neutron fluctuates around zero and nowhere exceeds ten percent. The effect on the angular distribution is to overestimate the 16-degree cross section by approximately 0.25%. Thus the angular resolution errors are small.

Since air scattering amounts to about 5%/m at 0.025 ev and since the sample to detector flight paths are in air, it might be expected that the outgoing beam of scattered neutrons would be further scattered in the air and some either miss the detector bank or be scattered into another detector bank. From the standpoint of a

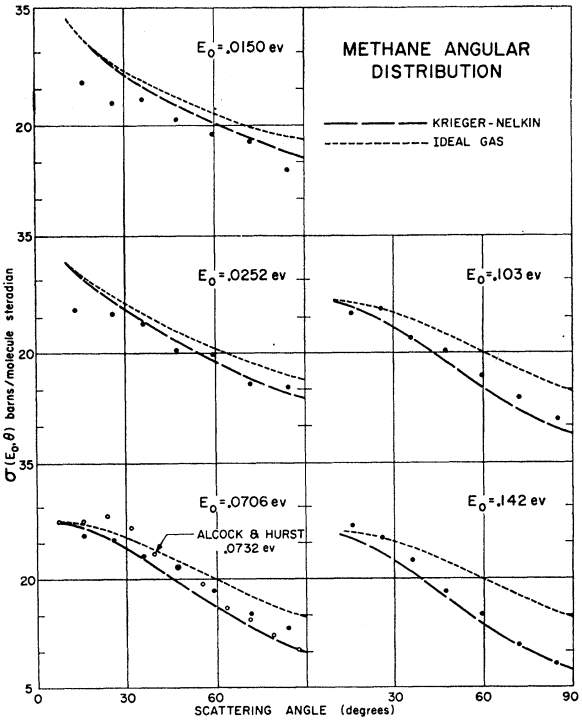

FIG. 8. Angular distributions of methane. Both theoretical cross sections are calculated using an effective mass of $M = 3.2$ hydrogen atoms per hydrogen scatterer, and do not include any contributions from the carbon.

given counter bank the effect of such secondary scattering is the net result of those neutrons scattered into it from other directions minus those scattered out. A measurement of this effect was made using a cadmium collimator, which subtended the entire solid angle defined by one counter bank and extended from the sample to the counter bank. Time-of-flight spectra in this bank for scattered neutrons were compared with those of the adjacent uncollimated bank. This comparison was made with and without the collimator in place. The presence of the collimator had no noticeable effect on either spectrum, indicating that air scattering of the scattered beam was negligibly small for this experiment.

Angular distributions $d\sigma/d\Omega$ were obtained by integrating the partial differential cross sections over the scattered neutron wavelengths. These are shown in Fig. 8 for 0.0150-, 0.0252-, 0.0706-, 0.103-, and 0.142-ev incident neutron energies. Also in the figure are shown the data of Alcock and Hurst[6] at 0.0732 ev and 5 atm pressure. Since their distribution was not absolute it was normalized to this experiment, the angle of normalization being 47°.

IV. SCATTERING LAW

A. Scattering Law Presentation

The partial differential cross sections obtained from a given sample are functions of three neutron variables, the incident and scattered neutron energies E_0, E, and the neutron scattering angle. The cross sections are also functions of parameters of the scatterer such as its mass and physical state, as well as the sample temperature. Egelstaff[11] has proposed for polycrystals, liquids, and gases a dimensionless form of presentation of such cross sections, called the "scattering law," in which the number of explicit variables is reduced to two: the square of the neutron momentum change $\hbar Q$ and the neutron energy change ΔE in dimensionless units. The neutron momentum change and the neutron energy change are the variables most commonly encountered in theoretical considerations of scattering. The Egelstaff scattering law, hereafter called ESL, contains only the dynamics of the molecular system, the nuclear effects being removed as well as the detailed balance factor.

The partial differential cross section for neutron scattering is written[11] in terms of the Egelstaff scattering law expression, $S(\alpha,\beta)$:

$$\sigma(E_0,E,\theta)=[\sigma_b/(4\pi k_BT)](k/k_0)\exp(-\beta/2)S(\alpha,\beta),$$
$$\alpha=\hbar^2Q^2/(2Mk_BT), \quad \mathbf{Q}=\mathbf{k}-\mathbf{k}_0, \qquad (1)$$
$$\beta=\hbar\omega/(k_BT), \quad \hbar\omega=E-E_0,$$

where E_0, $\mathbf{k}_0$, E, and $\mathbf{k}$ are the energy and wave vector of the incident and scattered neutrons, respectively. The variable θ is the laboratory scattering angle, σ_b is the bound total cross section of the scattering nucleus, and the constant M is a mass.

The convention used here is that β is chosen positive for neutron energy gain. Schofield[15] has shown that $S(\alpha,\beta)$ is even in β and Q. As a consequence of the evenness of $S(\alpha,\beta)$ with respect to β, an experimental ESL must be independent of the sign of the energy transfer β. An important advantage of the ESL is that it allows presentation of a large amount of data in a compact form. The reduction from $\sigma(E_0,E,\theta,M)$ to the variables $S(\alpha,\beta)$, however, is accompanied by the disadvantage that for a given temperature α and β are not independent variables, i.e., $\alpha=[m/(Mk_BT)]\{2E_0+\beta k_BT-2[E_0(E_0+\beta k_BT)]^{\frac{1}{2}}\cos\theta\}$ where m is the neutron mass.

The mass M used in the definition of α, hereafter called the "effective mass," can be chosen arbitrarily. The value has been chosen here to compare the experimental results with the ideal gas theory. Theoretical values for such an effective mass can be obtained from theories using the mass tensor approximation[8–10] and involve this mass in the partial differential cross section. It should be noted that having chosen an effective mass to convert experimental cross sections to the ESL, any comparison of theory with experiment using the ESL introduces this effective mass via α whether or not the theoretical partial differential cross section involves it. However, for a theory not based explicitly on an effective mass, this introduction merely establishes the α scale used in comparing the theory to experiment and contains nothing physical.

B. Scattering Law Results

The ESL for methane was obtained by inverting Eq. (1) for fixed values of the energy transfer β. This inversion uses the cross section in the form differential in neutron energy and scattering angle, and is done on a computer. For a given scattering angle and energy change β, the value of the cross section used to compute $S(\alpha,\beta)$ is obtained by an interpolation which fits a parabola to the two nearest data points on both sides of the energy of interest. This procedure thus takes into account curvature in the partial differential cross section and is more consistent than the method of hand-drawing a smooth curve through the data, as well as being faster.

The results for representative values of β are shown in Fig. 9. $S(\alpha,\beta)$ values are per molecule and include the carbon contributions. The mass M in the definition of α, used in converting the experimental partial differential cross sections to ESL, was chosen here to be 3.2 hydrogen atomic masses. This "effective mass" is obtained using the Sachs-Teller mass tensor[8] (see also Sec. V). The value of k_BT used in defining α and β is 0.02533 ev or 294°K. For $M/m=3.2$, the reduced neutron wave vector change is $Q=6.25\alpha^{\frac{1}{2}}$ (A)$^{-1}$. The data are shown so as to display the range of momentum transfers α obtained with a given incident energy. The lowest incident energies cover the lowest range of the α scale and for a

[15] P. Schofield, Phys. Rev. Letters 4, 239 (1960).

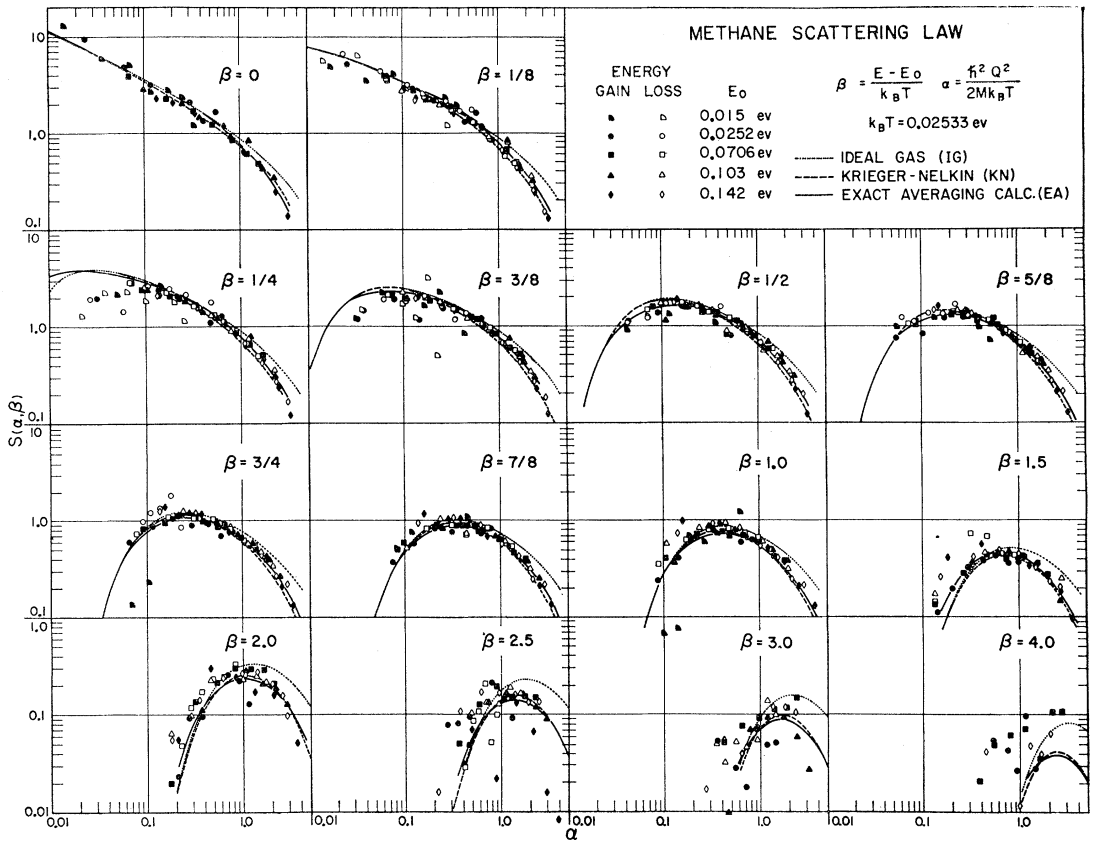

FIG. 9. Methane scattering law. The value of $S(\alpha,\beta)$ is per molecule, and the effective mass used to convert the partial differential cross sections to $S(\alpha,\beta)$ is $M=3.2$ hydrogen atomic masses.

fixed incident energy, the smaller the scattering angle, the smaller the value of α. Generally, there is an overlap of data obtained from different incident energies, so that the ESL intermixes data from different incident energies and scattering angles, and is thus overdetermined experimentally.

Since the general theory of the ESL shows that $S(\alpha,\beta)$ is even in β, there should be no splitting of experimental $S(\alpha,\beta)$ points into $+\beta$ and $-\beta$ branches for a given $|\beta|$. This furnishes a valuable internal check on the consistency of the data. Such systematic errors as incorrect measurements of neutron flight distances, time-of-flight measurement errors, incorrect background subtraction, the wrong sample temperature or large multiple scattering effects can cause an experimental $S(\alpha,\beta)$ curve to split. In the methane experimental ESL, no evidence of consistent splitting is present. Figure 10 shows the combined experimental scattering law for methane for comparison. These curves are hand-drawn best fits to the data shown in Fig. 9.

As a check on the accuracy of the counter calibrations, the cross section data of the experiment were compared with the total cross section at 0.025 ev obtained by Melkonian.[5] To do this, data were needed for back-angle scattering. These were obtained using the ESL results. The curves of Fig. 10 were used to regenerate partial differential cross sections, using Eq. (1), at 0.025 ev for angles greater than 90° as well as for the forward angles. These were then integrated over energy and angle to obtain the total cross section. The value obtained was 8% higher than Melkonian's. Since this experiment was not specifically designed to measure total cross sections, it was felt that Melkonian's value was more reliable. The data shown in Figs. 2–10 are normalized to agree with Melkonian.

V. COMPARISON OF THE THEORY WITH EXPERIMENT

The theory of slow neutrons scattered from gases has been studied by several authors. In each of these the Fermi pseudopotential is used to calculate the nuclear part of the scattering in first Born approximation. The mass-tensor approximation[10] has been used to treat classically the molecular rotations[9,10] and extended to include vibrations.[8,9] Zemach and Glauber[7] have given a theory for molecular scattering, whose formalism does not use the mass tensor or other approximations. Three calculations are compared with the data of this experiment. In each of these the rotations of the molecule are treated classically.

1. The Exact Averaging Calculation (EA)

This is a calculation[12] which treats the rotations classically but is calculated by the ZG formalism. No approximations are used in the thermal orientation averaging of either the rotational or the vibrational matrix elements. However, the assumption is made in the Hamiltonian that the rotational, vibrational, and translational effects may be separated. This calculation is for incident neutron energies below the first vibrational state and for energies large compared to the rotational level spacing, but includes the effects of zero point vibrations. It also includes the carbon contributions as well as the C-H, H-H interference effects in a given molecule.

2. The Krieger-Nelkin Theory (KN)

This[9,12] uses the mass-tensor (classical) approximation to the ZG formalism. It is valid for incident energies below the first vibrational state. In this, approximations are made in the orientation averages of both the rotational and the elastic vibrational matrix elements. The mass tensor arises in treating this average in the rotational matrix element. The effective mass used in Fig. 9 is $M/m=3.2$ rather than the KN value of 3.4. This effective mass is the reciprocal of the average of the trace of $\mathfrak{M}^{-1}$, the Sachs-Teller[10] mass tensor. The KN theory in ESL form is given by

$$S(\alpha,\beta)=4/(4\pi\alpha)^{\frac{1}{2}}\exp[-(\alpha^2+\beta^2)/4\alpha-K(M)\alpha],$$

where $K(M)=2Mk_BT\gamma/\hbar^2$ is the zero-point vibrational factor and γ (for this case) is a constant depending on the vibrational levels of the molecule. For $M/m=3.2$, $K(M)$ is equal to 0.246. The factor 4 in front of this expression is to account for the four hydrogen atoms per molecule. This expression does not include interference effects or the scattering from carbon. The KN calculation yields total cross sections for methane in agreement with experiment.[9]

3. Ideal Gas (IG)

The theoretical expression for scattering from an ideal gas can be obtained by setting the vibrational exponential factor in the KN theory equal to one. In the limit of a rigid molecule, this factor actually becomes one and the expression for $\sigma(E_0,E,\theta)$ in the KN theory corresponds to scattering from a monatomic gas having an effective mass 3.2. For this case the ESL does not then depend explicitly on the effective mass, though computed partial differential cross sections do.

The solid curves shown in Figs. 3–7 are the partial differential cross sections obtained from the EA calculation. There is no normalization of these theoretical curves to the data. Generally, for the 0.07-, 0.1-, and 0.14-ev data (Figs. 5–7) and for all except the two most forward angles of the 0.025- and 0.0150-ev data, the theory agrees with the experiment as to magnitude and as to shape. The most significant disagreement is for the angles of 16° and 26° at 0.0252 and 0.0150 ev (Figs. 3 and 4) where the theories are lower and broader than the experiment. Also the theoretical cross sections at these angles are shifted to shorter wavelengths than the experiment. The theoretical curves shown here have not been broadened by instrumental resolution, the effect of which would be to make the disagreement slightly larger.

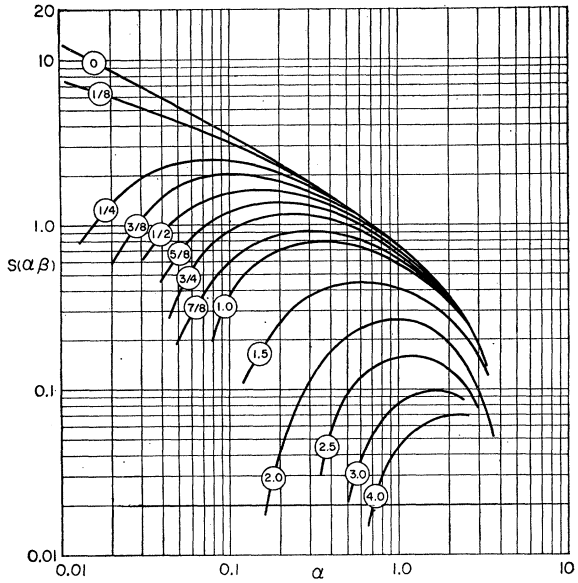

FIG. 10. Combined methane scattering law. These curves are hand-drawn best-fit curves to the data of Fig. 9. The circled numbers on each curve are the values of β. Temperature=21°C. Effective mass $M=3.2$ hydrogen atoms per hydrogen scatterer. $\beta(0.0253\text{ ev})=1$.

For the angular distributions (Fig. 8), both the IG and KN are larger than experiment at 0.015 and 0.025 ev. At 0.07, 0.1, and 0.14 ev the IG is higher and the KN is lower than the experimental cross sections. For these energies KN gives the better fit. At all the energies the EA angular distribution is not significantly different from the KN and is therefore not shown.

For the scattering law (Fig. 9), generally, the ideal gas and KN theory bracket the data for α values above the maximum of the experimental scattering law. The KN theory agrees somewhat better than the ideal gas. The EA calculation agrees best in this region of α for the intermediate values of β. At small α all three calculations give about the same results for ESL. In this region all the theories show a deviation from experiment. In particular, there are large deviations at small α, for β lying between $\frac{1}{8}$ and $\frac{5}{8}$ and again for $1\lesssim\beta\lesssim4$. These deviations would not be expected to be caused by effects due to coherent scattering since the dominant scatterer is hydrogen. This is borne out by comparison with EA which includes interference effects. Also, since the gas is at a low density no coherence due to molecular long-range order is expected.

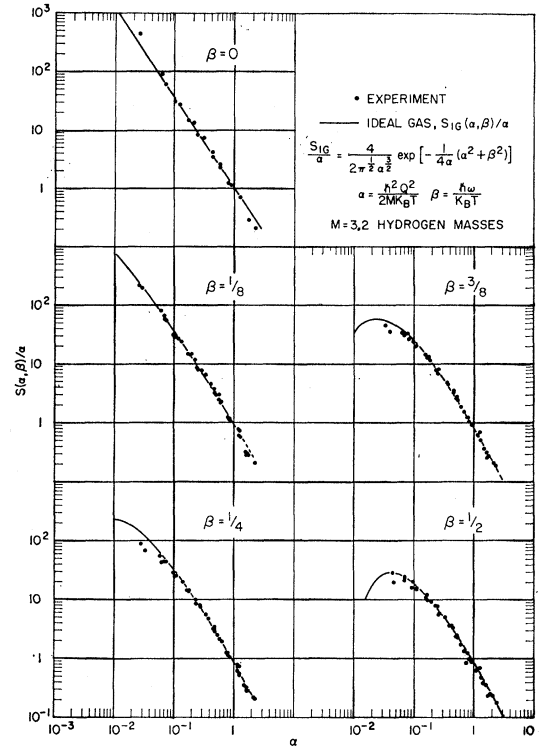

FIG. 11. Typical plots of $(1/\alpha)S(\alpha,\beta)$ vs α for methane. For α approaching zero the ideal gas curve yields zero for all β values except $\beta=0$, where S/α becomes infinite.

A change in effective mass does not affect the relation between the EA calculation and the data since such a change merely shifts the theory and experiment by the same amount on the α scale, in Fig. 9. For the IG, however, an effective mass of approximately 2.6 (which shifts the scattering law data to larger α with respect to the IG curve) yields a much better fit of IG for $\beta \gtrsim \frac{3}{4}$ over the whole range of α. On the other hand, for β less than $\frac{3}{4}$ the fit becomes worse. For the KN theory, using an effective mass of 2.6 makes only a very slight improvement at large α, not nearly so much as it does for IG, and it also increases the disagreement at low α. Using the KN effective mass 3.4 rather than the 3.2 obtained from Sachs-Teller slightly increases the discrepancy ($\sim$6%) at all α and β. From these fits an ideal gas of mass 3.2 can be said to give a rough fit for $\alpha \gtrsim \frac{3}{8}$, while the KN with mass 3.2 gives a better fit in this α range. Generally however, especially for $\beta<1$, EA gives the best fit over the largest α range.

The low points in the scattering law occurring for β between $\frac{1}{8}$ and $\frac{5}{8}$ arise from data obtained at the two forwardmost angles, 16.3° and 26.0° from the 0.015- and 0.025-ev incident energies (Figs. 3 and 4). Were there serious systematic errors in the calibration of the counters at these angles or in the determination of other experimental parameters such as time-of-flight or the distance of neutron flight, they would occur also for all β values and for all incident energies. The experimental ESL shows no evidence of this. The disagreement between the theories and the data is probably due to the discrete spacing of the rotational levels, which are treated as continuous by the three calculations. At large β values none of the theories agree with the experiment either as to magnitude or shape for the effective mass of 3.2. Here, however, especially at 0.14 ev, contributions from the effect of the first vibrational state at 0.16 ev may be occurring which were not included in these theories. Also for $\beta \gtrsim 1$ the signal to background ratio is very small, being only of the order of 1.1 to 1.5.

The conclusion drawn is that the basic cause of the disagreement with the experiment at small momentum transfers and intermediate energy transfers is that the treatment of the molecular rotations classically is inadequate. The correct orientation averaging procedures used in EA, though an improvement for large momentum transfers, is not an improvement for small α and β.

It has been shown by Egelstaff[11] that the coefficient of self-diffusion for a material may be obtained by extrapolating the incoherent part of the scattering law. The relation given is $[\pi\beta^2(S/\alpha)_{\alpha\to 0}]_{\beta\to 0}=2MD/h+O(\beta^2)$, where D is the coefficient of self-diffusion of the material and M the mass of an atom in the system. For this experiment, since hydrogen is an incoherent scatterer, the complete scattering law can be used. In order to obtain the diffusion coefficient, which is a characteristic of the long time behavior of the system, $(S/\alpha)_{\alpha\to 0}$ is extrapolated first, then $[(S/\alpha)_{\alpha\to 0}]_{\beta\to 0}$. Figure 11 shows plots of S/α vs α for representative values of β. The solid curves shown are for the ideal gas, which in the region of small α is not significantly different from either the KN theory or the EA calculations. It is seen that in order to extrapolate α to zero with any accuracy, data at much smaller α will be needed. If the extrapolation is made to follow the ideal gas curve, a delta function in β results which would yield an infinite diffusion coefficient as expected for an ideal gas.

VI. SUMMARY AND CONCLUSIONS

By presenting the scattering data as ESL (which intermixes data from different initial energies and angles), in the regions of overdetermination the sources of experimental error such as resolution, backgrounds, errors in distance or time, etc. are evident and can be eliminated or corrections can be made. Also, from a few initial neutron energies sufficient information is available to generate partial differential cross sections for many initial neutron energies. This is important in programs for calculating reactor spectra where it is impossible to store in a computer the partial differential cross sections for all initial neutron energies needed. The scattering law also guarantees through the detailed balance factor that the neutron spectra will reach a Maxwellian in large nonabsorbing media.

Comparison of the data with the three theoretical calculations show that the classical treatment of the rotations used in these calculations does not explain the data at small momentum and energy transfers. At large momentum transfers where vibrational states become important the EA treatment, which treats the orientation averages exactly, gives the best fit. For generating partial differential cross sections to be used in reactor calculations, the simpler but less accurate IG or KN theories may be satisfactory for a simple material like methane. Only more experience in comparing measured reactor parameters that are sensitive to the inelastic scattering, such as the transport cross section or the diffusion lengths, to values calculated using the experimental data and to those obtained using the less accurate theories, will answer this question.

ACKNOWLEDGMENTS

We are much indebted to Dr. G. W. Griffing and Dr. H. L. McMurry for many helpful discussions and calculations of theory and to Dr. C. A. Coombes for help in the early stages of data analysis. Our thanks are also given to Mrs. C. J. Slayden who did the data analysis computations and wrote most of the programs used, and to R. B. Kennedy for technical assistance. We also wish to thank Dr. J. E. Evans and Dr. R. G. Fluharty for their continued advice and encouragement during the course of this experiment.